nature communications

Article

https://doi.org/10.1038/s41467-024-54785-y

The glycerol stabilized calcium phosphate cluster for rapid remineralization of tooth enamel by a water-triggered transformation

Received: 1 December 2022

Accepted: 21 November 2024

Published online: 02 January 2025

Check for updates

Nan Luo[1,2,3,4,5,11], Bing-Qiang Lu[6,11] ✉, Yu-Wei Deng[2,3,4,5,7,8], Hua Zeng[6], Yu Zhang[1,2,3,4,5], Jing-Yu Zhan[1,2,3,4,5], Xiao-Chen Xu[1,2,3,4,5], Gui-Zhi Cao[2,3,4,5], Jin Wen[2,3,4,5,7,8], Zhiyuan Zhang[2,3,4,5,9], Xi-Ping Feng[1,2,3,4,5], Xinquan Jiang[2,3,4,5,7,8], Feng Chen[6,10] ✉ & Xi Chen[1,2,3,4,5] ✉

Remineralization is a common strategy for the repair of early demineralized tooth enamels, but the harsh dynamic oral environment often hampers its efficacy. Rapid remineralization is expected to address this challenge, however, the stabilizers of remineralization materials often resist their transformation required for repair. Here, by dissolving the ions of calcium and phosphate in glycerol-dominant solvents, we obtain the calcium phosphate clusters (1–2 nm), which are stabilized by glycerol (with high viscosity and affinity to clusters), but can perform a fast enamel repair via the water-triggered transformation in both static and dynamic environments. Upon the in vitro and in vivo (female Sprague-Dawley rats) studies, the clusters swiftly enter the nano-/micro-sized enamel defect sites, then form a compact hydroxyapatite repair layer within a short time (30 min, much faster than the conventional materials), and significantly recovers mechanical properties. This material is promising for large-scale preparation and applications in dental remineralization.

Loss of tooth tissues by demineralization or trauma is one of the most negative factors on life quality, causing health problems and economic burdens throughout the world[1]. As an outstanding biomineralization work in nature, human tooth enamel forms via a programmed series of cellular and biochemical regulations[2]. Due to the irreproducible enamel development microenvironment after tooth eruption, enamel is scarcely self-repaired if damaged[3,4]. For example, the cavity caused by dental caries normally progresses continuously without reverse, and ultimately impairs underlying dentin, even the pulp. Until now, a variety of materials such as fluoride[5], casein phosphopeptide (CPP)[6], amelogenin mimics[7] and calcium phosphates[8,9] have been explored to remineralize enamels by promoting the growth of fluor-/hydroxyapatite (HAP). Generally, a complex procedure of pre-treatment and a mild static environment during treatment are required to achieve an

[1]Department of Preventive Dentistry, Shanghai Ninth People's Hospital, Shanghai Jiao Tong University School of Medicine, Shanghai, PR China. [2]College of Stomatology, Shanghai Jiao Tong University, Shanghai, PR China. [3]National Center for Stomatology, Shanghai, PR China. [4]National Clinical Research Center for Oral Diseases, Shanghai, PR China. [5]Shanghai Key Laboratory of Stomatology, Shanghai Research Institute of Stomatology, Shanghai, PR China. [6]Center for Orthopedic Science and Translational Medicine, Department of Orthopedic, Spinal Pain Research Institute, Shanghai Tenth People's Hospital, School of Medicine, Tongji University, Shanghai, PR China. [7]Department of Prosthodontics, Shanghai Ninth People's Hospital, Shanghai Jiao Tong University School of Medicine, Shanghai, PR China. [8]Shanghai Engineering Research Center of Advanced Dental Technology and Materials, Shanghai, PR China. [9]Department of Oral and Maxillofacial-Head Neck Oncology, Shanghai Ninth People's Hospital, Shanghai Jiao Tong University School of Medicine, Shanghai, PR China. [10]Shanghai Key Laboratory of Craniomaxillofacial Development and Diseases, Stomatological Hospital and School of Stomatology, Fudan University, Shanghai, PR China. [11]These authors contributed equally: Nan Luo, Bing-Qiang Lu. ✉e-mail: bqlu@tongji.edu.cn; chen_feng@fudan.edu.cn; cherry_cxnet@sjtu.edu.cn

ideal outcome. Despite this, the repair efficacy of these materials is still weakened by low rate. For example, the tooth interface should be dried first, then coated with the materials followed by being dried again, and finally incubated in static artificial saliva for a long time to induce transformations of the applied materials or the precipitation of apatite crystals[7,8,10]. The real oral environments, in contrast, are much harsher since the sustained flow of liquid in the mouth and friction on the tooth surface may lead to the detachment of materials from enamels before finishing the repairs. Therefore, a rapid repair rate in harsh dynamic environments is desired to avoid or diminish these influences for more effective enamel remineralization.

The human tooth enamel is highly patterned and consists of tightly packed arrays of HAP nanorods that organize into an intricate interwoven structure[3]. While originating from calcium and phosphate ions, the HAP formation in solutions involves various intermediate species ranging from pre-nucleation ones (e.g., prenucleation cluster[11–13], liquid precursor[14,15], ion dense liquid[16]) to post-nucleation ones (e.g., amorphous nanocluster[17,18], amorphous nanoparticle[19], nanocrystal[20,21]). Theoretically, each one can be potentially used to build the target complex structures. In fact, it is believed that their formation, growth, assembly and phase transformation are tuned by cells and secreted substances in animals to form the hard tissues with delicate structures and strong mechanical properties[3,22]. This has inspired researchers to repair the enamel defects based on specific intermediate species[8,23–25], but the resultant structures are often distinct from native enamels, or the repair process takes long time due to low transformation rates. For a rapid remineralization, the used materials should quickly adhere to the enamel surface, then permeate into the nano-/micro-sized interstices, and transform into HAP nanorods in saliva within a short time. However, a dilemma arises: stabilizers are required to capture the intermediate state during synthesis and storage of these materials, but their transformations are unexpectedly inhibited by stabilizers when treating enamel defects.

In this study, we have developed an intermediate species of mineralization in the glycerol-dominant solvents (major glycerol and minor water), denoted as glycerol stabilized calcium phosphate cluster (GCPC), to address this challenge. Glycerol is widely used in biomedicine, food industry, cosmetics and oral products owing to remarkable biocompatibility[26,27]. With high molecular polarity, glycerol is able to solubilize a variety of polar molecules and inorganic salts. Besides, given its big size, high viscosity and affinity to various cations (e.g., Ca^{2+}) via the ternary-hydroxy groups, glycerol can effectively retard the transformation and aggregation of the metastable substances formed in it, which is beneficial for obtaining the early state species during their evolution. However, the calcium phosphate cluster has never been explored in glycerol (or glycerol-dominant solvents) and other non-toxic organic solvents before, to the best of our knowledge. As for GCPC, water molecules rapidly exchange with glycerol in aqueous environments (e.g., saliva), disturbing the stability of the GCPC, finally inducing assembly and transformation. Indeed, our studies find that, GCPC, with a very small size (1–2 nm) and high stability in the glycerol-dominant solvents, is able to remineralize the acid etched enamels rapidly in a water-triggered way: on enamel, it can easily enter the nano-/micro-sized defect sites and transform into HAP nanorods immediately. Both in vivo and in vitro, GCPC restores enamel mechanical properties by forming a dense mineral repair layer in static or dynamic saliva. This character effectively avoids the impact of the dynamic environments in oral, which provides an enlightening foundation for the efficient repair of damaged enamels.

Results

The preparation and characterization of GCPC

GCPC was obtained in a solution of Ca^{2+} and PO_4^{3-} ions dissolved in the glycerol-dominant solvents (major glycerol and minor water). As a polar solvent, glycerol is able to dissolve Ca^{2+} and PO_4^{3-} salts, but inhibits their reaction into calcium phosphate precipitations, which differs from water solvent. Indeed, as shown in Fig. 1A, the glycerol solution containing 0.050 mol/L Ca^{2+} and 0.033 mol/L PO_4^{3-} ions displays very weak turbidity and its OD value has no significant difference from that of pure glycerol (Supplementary Fig. 1), indicating that rare mineral species are yielded, which is varied from the manifest white precipitation formed in the aqueous solution. In addition, dynamic light scattering (DLS) measurement of the glycerol solution (Supplementary Fig. 2) shows that the size of the species in it is beyond the measurable range of instrument, indicating that PO_4^{3-} and Ca^{2+} mainly keep in the state of ions and other prenucleation species[28], but should be much less in the form of post-nucleation precipitation. When water is introduced into the glycerol solutions while maintaining the ion concentrations, it distinctly turns turbid (Supplementary Fig. 1A–C) and the turbidity is improved with the increase of water content (volume content of water in solvents is from 1.67 to 16.7 v/v%), consistent with the rise of the OD values (from 0.053 to 0.13) in Supplementary Fig. 1F. On liquid nuclear magnetic resonance (NMR) spectra (Fig. 1B), the solution of PO_4^{3-} ions (from Na_3PO_4) in the glycerol-dominant solvents (water content 16.7 v/v%) corresponds to a sharp resonance at 3.2 ppm, but a broader one in the range of −15 ~ 15 ppm arises along with the sharp one significantly weakened and shifted (to 2.8 ppm) when Ca^{2+} ions (from $CaCl_2$) are added. These all indicate that the solutions of Ca^{2+} and PO_4^{3-} ions form new species in the glycerol-dominant solvent. Besides, when tripling the concentration of Ca^{2+} and PO_4^{3-} ions (to 0.15 and 0.10 mol/L, respectively, termed 3X-GCPC), a more turbid (also higher OD value) but still stable solution is obtained (Supplementary Fig. 1D), where no significant phase separation is observed even under centrifugation speed of 11660.4 × g for 1 min, suggesting a high solubility of the formed species that correspond to the turbidity.

Liquid cell TEM is capable of in situ monitoring species in the solutions, which avoids the negative effects by the drying operation required for the conventional TEM observation[29]. This technology was applied to elucidate the morphology of the formed species in glycerol-dominant solvents. Here, the glycerol solution containing Ca^{2+} and PO_4^{3-} with volume content of water in solvents 16.7 v/v% and the size of the species in it were characterized using a spherical aberration corrected transmission electron microscope (ACTEM) equipped with a liquid cell holder. As shown in Fig. 1C, clusters with dark contrast in the size of 1–2 nm confirmed by DLS analysis in Supplementary Fig. 3) are observed (labeled with squares) in the solution, which are denoted as glycerol stabilized calcium phosphate clusters (GCPCs) due to the essential stabilizing effect by glycerol as in the following discussions. Previously, calcium phosphate clusters have been reported in aqueous[13] or organic solutions[30]. In general, bare clusters are extremely unstable and tend to aggregate into bigger particles or even chemically transform immediately after formation. Establishing stabilizers on their surfaces is required to avoid this, however, they may in turn impair the intended assembly and transformation of the clusters when building the target structures.

In our strategy, the aggregation and transformation of GCPC are effectively inhibited by glycerol, but can be triggered by replacing glycerol with a certain substance, e.g., water. Indeed, we find that the prepared GCPC shows very high stability. During observing GCPC with ACTEM in liquid cell, no morphological changes were found, which also corroborates that this species is not a byproduct of electronic beam irradiation. Besides, the GCPC solution (water content 16.7 v/v%) can keep a homogeneous state without visible phase separation for at least 2 weeks (Supplementary Fig. 1E). Liquid cell-ACTEM further reveals that the GCPC, after a storage at room temperature for 2 weeks, are still 1–2 nm sized clusters predominantly along with very fewer bigger particles, although their distributions in the solution become heterogeneous (weak aggregation) (Supplementary Fig. 4). However, when being dispersed in a large amount of water (1 mL GCPC in 10 mL

https://doi.org/10.1038/s41467-024-54785-y

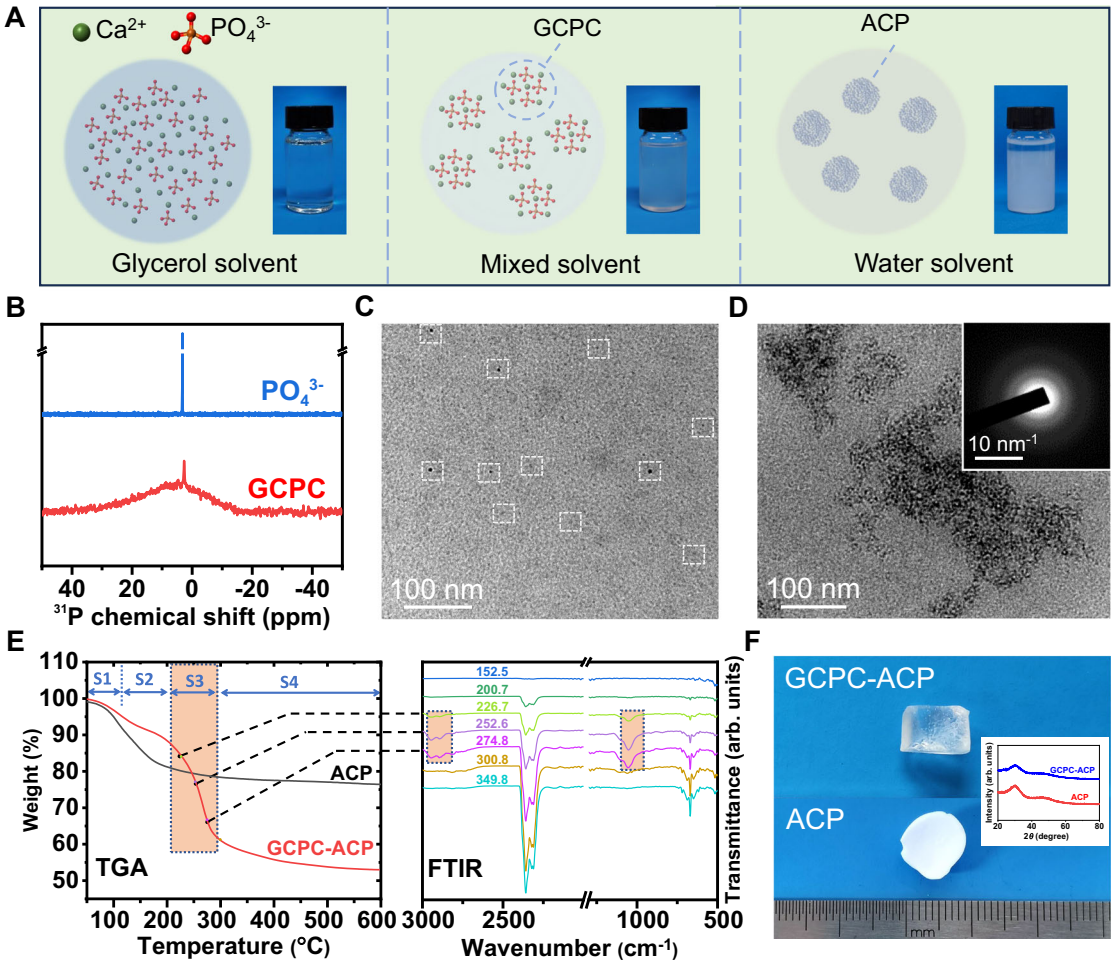

Fig. 1 | Synthesis and characterization of GCPC. A Schematic and digital images of the prepared solutions by adding the same concentration of PO_4^{3-}/ Ca^{2+} (0.033 and 0.050 mol/L, respectively) in different solvents (glycerol, mixed (glycerol + water, water content 16.7 v/v%) and water solvents). **B** ^{31}P NMR spectra of the solutions containing PO_4^{3-} ions or PO_4^{3-}/ Ca^{2+} ions in the glycerol-dominant solvent (deuterated water: 16.7 v/v%; glycerol and other chemicals are not deuterated). **C** Liquid cell TEM image of GCPC in the solution of glycerol-dominant solvent (water content 16.7 v/v%). White dashed squares highlight the GCPCs on the image. **D** TEM image of GCPC-ACP formed by adding GCPC into a large amount of ethanol. Inset: SAED pattern. **E** TGA-FTIR analysis of ACP and GCPC-ACP where FTIR spectra (right) of the gas released during heating the sample for TGA (left) is collected simultaneously. The TGA curve of GCPC-ACP displays four stages (labeled as S1-S4). The selected FTIR spectra (recorded at 226.7–274.8 °C as indicated on each spectrum) of S3 show characteristic bands at 2948, 2894 and 1054 cm^{-1} marked with rectangles, indicating that this stage corresponds to the loss of glycerol. Therefore, the contents of water and glycerol are calculated to be 8.37 wt% and 27.4 wt%, respectively. **F** Digital images of dried GCPC-ACP (top) and normal ACP (bottom) prepared in water displaying a high transparency and an opaque white, respectively. Inset: XRD spectra revealing the amorphous phases of GCPC-ACP and ACP.

water), where the glycerol exchanges with water molecules driven by the high miscibility of glycerol and water, precipitates are immediately formed, which turns out to be ACP nanoparticles according to TEM and selected area electronic diffraction (SEAD) characterizations (Supplementary Fig. 5). Such ACP will further crystallize in aqueous solutions as discussed below. The results suggest that, although possessing high stability, GCPC can undergo a rapid conversion by the induction from water, which is termed the water-triggered transformation in this paper.

When mixing GCPC with the solvents of different alcohols at a volume ratio of 1:10 to exchange glycerol with each of them, solid precipitation occurs immediately with those of low viscosity, but does not in higher ones (Supplementary Fig. 6). This experiment, although cannot exclude the effect of other effects (e.g., affinity between solvents and clusters), implies that the high viscosity of glycerol should contribute to stabilizing the clusters. The precipitation yielded by mixing GCPC with ethanol (denoted as GCPC-ACP) was characterized. As shown in Fig. 1D, it displays a morphology of aggregated clusters with amorphous phase (according to SAED pattern in Fig. 1D inset), which also corroborates the cluster morphology of GCPC. The size of GCPC-ACP (28.2 ± 4.9 nm) dispersed in ethanol was determined by DLS analysis (Supplementary Fig. 7), which is consistent with the TEM observations. Thermogravimetric-Fourier transform infrared spectrometric (TGA-FTIR) analysis (Fig. 1E) was used to further characterize GCPC-ACP, by which FTIR spectrum of the gas released during heating the sample for TGA is collected simultaneously. In addition to water (8.37 wt%), a high content of glycerol (27.4 wt%) is determined in GCPC-ACP as well, which is further confirmed by gas chromatography-mass spectrometry (GC-MS) (glycerol content: 21.2 wt%, Supplementary Fig. 8). As this sample was washed with ethanol for 6 times, and thoroughly dried in vacuum (only trace amount of ethanol remains in it, Supplementary Fig. 8), it is reasonable to speculate that, like water, glycerol molecules are incorporated in GCPC-ACP rather than weakly adsorbed on its surface. This also indicates that glycerol has a strong interaction with GCPC in the solvents, which thus contributes to their high stability. Interestingly, the dried GCPC-ACP displays a monolith state with a high transparency (Fig. 1F), which is different from the white color of normal ACP prepared in water and previously reported ACP powders[31], indicating a high structural continuity with the constituent particles highly compacted or fused[32].

https://doi.org/10.1038/s41467-024-54785-y

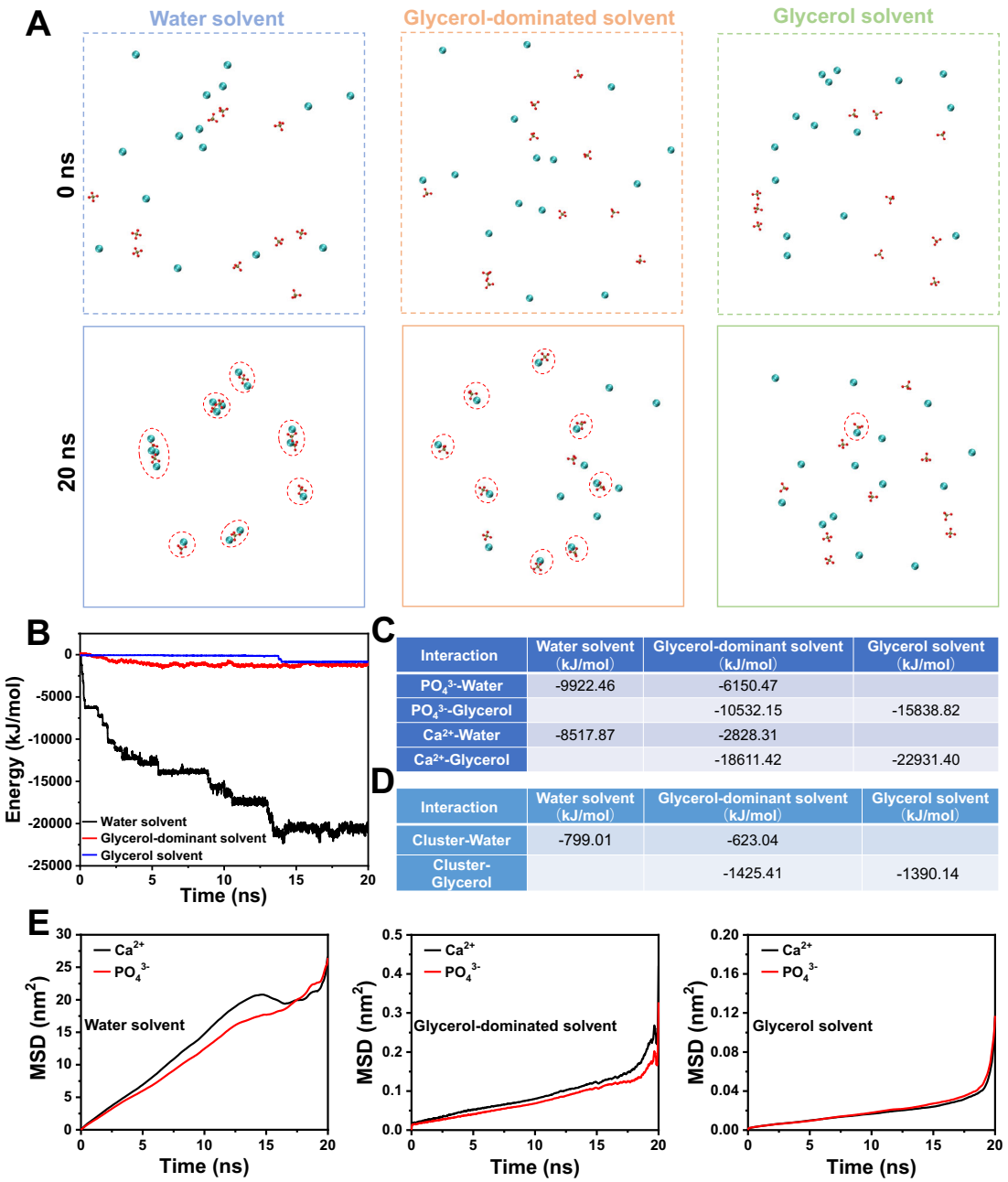

C

Interaction	Water solvent (kJ/mol)	Glycerol-dominant solvent (kJ/mol)	Glycerol solvent (kJ/mol)
PO_4^{3-}-Water	-9922.46	-6150.47	
PO_4^{3-}-Glycerol		-10532.15	-15838.82
Ca^{2+}-Water	-8517.87	-2828.31	
Ca^{2+}-Glycerol		-18611.42	-22931.40

D

Interaction	Water solvent (kJ/mol)	Glycerol-dominant solvent (kJ/mol)	Glycerol solvent (kJ/mol)
Cluster-Water	-799.01	-623.04	
Cluster-Glycerol		-1425.41	-1390.14

Fig. 2 | Molecular dynamic simulations on the evolution of calcium phosphate cluster. The simulation starts from dissolved ions in water solvent, glycerol-dominant (glycerol + water, water content 16.7 v/v%) and glycerol solvent. **A** Snapshots of the spatial distributions of ions and formed clusters (marked with dashed circles) at 0 ns and 20 ns. Solvent molecules are omitted for clarity. Atoms Ca, P and O are shown in blue, brown and red, respectively. **B** Interaction energy between Ca^{2+} and PO_4^{3-} ions in water, glycerol-dominant and glycerol solvent. **C** The average interaction energy between Ca^{2+} or PO_4^{3-} with glycerol or water in the solvents at the beginning 0–2 ns. **D** The average interaction energy between a primary cluster (constituted by one Ca^{2+} and one PO_4^{3-}) and solvent molecules in the time range of 15–20 s. **E** The mean square displacement (MSD) of Ca^{2+} and PO_4^{3-} in water, glycerol-dominant and glycerol solvents.

Molecular dynamics simulation of the GCPC formation

A molecular dynamic simulation (Fig. 2) was conducted to further analyze role of glycerol on both the formation and stabilization of GCPC. Such simulation is based on the evolution of calcium phosphate cluster in the glycerol-dominant solvent (water content 16.7 v/v%, same as GCPC preparation) with those in pure water and pure glycerol solvents as the controls. Due to the limited computation time, the clusters displayed here should correspond to their early states instead of the mature ones. However, we can still observe the differences of the species and interactions in the different solvent systems, which already reveals the influence of the glycerol on them.

First, glycerol retards the formation of clusters in the solvents. Fig. 2A shows the spatial conformation of Ca^{2+} and PO_4^{3-} ions in three solution systems at start (0 ns) and end (20 ns) of simulation. At the initial stage of simulation, Ca^{2+} and PO_4^{3-} ions in all solvents are randomly distributed in the solvent. Over time, their reactions differ in different solvent systems. In water solvent, all Ca^{2+} and PO_4^{3-} ions are coordinated together to form clusters with various numbers of constituent ions (from 2 to 4) after 20 ns. In the glycerol-dominant solvent, most of the ions form the primary clusters (constituted by one Ca^{2+} and one PO_4^{3-}) without further aggregation into larger ones. However, only one primary cluster is obtained in glycerol solvent at the end, and the

other ions are still distributed in the solvent box in an uncoordinated state.

Second, glycerol weakens the interaction between Ca^{2+} and PO_4^{3-} in the solvents. The interaction energy between Ca^{2+} and PO_4^{3-} in these systems were further assessed throughout the simulation. It can be found in Fig. 2B that the interaction energy (absolute value) between Ca^{2+} and PO_4^{3-} ions in water solvent consistently rises within 15 ns, along with the continuous formation and aggregation of calcium phosphate clusters. In the glycerol-dominant solvent, the interaction energy has an increase before 6 ns when clusters forms, followed by gradual stabilization with minor fluctuations. The interaction energy in glycerol solvent does not exhibit significant change before 13 ns, and only an increase occurs between 13–15 ns upon the cluster formation, which then comes to stable again. Besides, comparing the final interaction energy between Ca^{2+} and PO_4^{3-} in these three solvent systems, the highest value is in water solvent (~-21,000 kJ/mol), followed by in glycerol-dominant solvent (~−1200 kJ/mol), and lowest in glycerol solvent (~−900 kJ/mol). This result indicates that glycerol can significantly reduce the interaction between the Ca^{2+} and PO_4^{3-}, which is also consistent with the retarded formation and aggregation of the clusters demonstrated above. Such reduction could be attributed to the varied interaction between ions and solvent molecules in different. As shown in Fig. 2C, at the beginning of 0–2 ns when the ions are mostly free in the solvents, either Ca^{2+} or PO_4^{3-} has a stronger interaction with glycerol than that with water.

Third, glycerol enhances the interaction between clusters and solvents. We chose a primary cluster formed before 15 ns in each solvent system with the same constituents and without aggregation before 20 ns, then comparing its interactions with different solvent molecules by averaging the energy in the time range of 15–20 s. As shown in Fig. 2D, the interaction energy between cluster and water is −799.01 kJ/mol in water solvent, while that between cluster and glycerol in glycerol solvent is −1390.14 kJ/mol, indicating that glycerol has a stronger interaction with the primary clusters than water, which thus have impacted their further aggregation.

Fourth, glycerol reduces the mobility of the ions in the solvents. The mean square displacement (MSD) as a function of time reveal dynamics of the ions in solutions systems and reflect the influence of solvent properties (e.g., viscosity) on it. As shown in Fig. 2E, Ca^{2+} and PO_4^{3-} ions in water solution have the highest MSD values, followed by those in glycerol-dominant solvents and then pure glycerol. Accordingly, Ca^{2+} and PO_4^{3-} ions have the highest diffusion coefficient 0.205 nm^2/ns and 0.192 nm^2/ns in water, respectively, and those in glycerol-dominant solvents are 0.0012 nm^2/ns and 0.0011 nm^2/ns. The lowest diffusion coefficient of Ca^{2+} (0.00025 nm^2/ns) and PO_4^{3-} (0.00030 nm^2/ns) are found in glycerol solution. Hence, glycerol does not favor the movement of ions in it, which in turn reduce their reaction towards the formation, growth and aggregation of clusters.

Repair of the demineralized enamel in vitro

GCPC was further applied in enamel remineralization to explore its application in dentistry. Here, GCPC in the glycerol-dominant solvents (termed GCPC solution or 3X-GCPC solution as described in experimental section), where it forms, was directly used for the studies. In our study, GCPC is advantageous in three aspects: (1) highly concentrated constituent ions of calcium phosphate in the solution (e.g., up to Ca^{2+} 0.15 mol/L, PO_4^{3-} 0.10 mol/L for the 3X-GCPC solution, comparing to 0.001–0.002 mol/L of them in (simulated) body fluids), without forming visible phase separation; (2) high fluidity and permeability endowed by its small size; (3) high stability and water-triggered transformation favoring both long-term storage and rapid repair.

Cytotoxicity of GCPC was first tested upon human oral keratinocytes (HOKs) and human dental pulp stem cells (DPSCs) with CCK-8 assay and live/dead staining. For each kind of cell (HOKs or DPSCs), the CCK-8 assay shows very little difference of the cell proliferations between the GCPC group (incubation of cells with GCPC) and control (incubation of cells without GCPC or other materials) after 1 d and 2 d (Supplementary Fig. 9A, B). The GCPC exhibits prominent biocompatibility even at a high concentration (50 mg/mL). The live/dead staining experiment further confirms the results, showing that both HOKs and DPSCs have high viability at 2 d in different concentrations of the GCPC (Supplementary Fig. 9C). Since glycerol, Ca^{2+} and PO_4^{3-} are rich in the human bodies, it is reasonable to understand the biocompatibility of GCPC, which is also essential for its applications in biomedicine.

Human tooth samples (premolars and third molars without caries) extracted for clinical reasons (orthodontic treatment or removal of impacted third molars) were used for study. A caries model was made by etching the sound tooth enamel with 37 wt% phosphoric acid for 60 s. SEM micrographs show that the smooth surface of sound enamel (Supplementary Fig. 10) changes into rough and porous with HAP nanorod crystals loosely arranged on it resulted by HAP dissolution in acid environment (Fig. 3A1–A3). The remineralization of enamel was subsequently demonstrated on this model caries. After totally wetting the etched enamel by artificial saliva (without additional drying as in other reports), a drop of GCPC solution was added onto it using a micro brush (brushing for 5 s) (Scheme Fig. 3B3), then immediately immersed in artificial saliva and incubated for 30 min or 24 h. Owing to the small size, GCPC can easily enter the nano-/micro-sized interstices of the defects (Fig. 3B1, B2). Afterward, they rapidly assemble and transform so as to remineralize the defects during the dissolving of glycerol in artificial saliva. At 5 min, SEM micrographs (Fig. 3C1–C3) show that the newly formed materials, which should be originated from GCPC in artificial saliva, densely fill in the defect sites at a very early stage (5 min). The results of SEM from the top and cross-sectional view reveal that the materials are composed of ACP nanoparticles and nanowires adhered on enamel crystals and their top ends. On some occasions, very well-defined ACP nanowire (diameter of up to tens of nanometers and length of up to hundreds of nanometers) with high aspect ratio can be found (inset of Fig. 3C1 and Supplementary Fig. 11). We also confirm the morphology of nanowires by TEM micrograph (Supplementary Fig. 12), the amorphous phase by the SAED pattern (inset of Supplementary Fig. 12) and the elementary composition of calcium phosphate by energy dispersive spectroscopy (EDS) (Supplementary Fig. 13). Over incubation time (10 min), a complete and uniform mineral layer can be observed on enamel surface, which should be derived from the fused ACP nanoparticles and nanowires (Fig. 3D1–D3). According to our observation, the ratio of ACP nanowires in the repair layers is much lower than that of nanoparticles. Hence, their contribution to the enamel remineralization is also much less. Besides, we note that the enamel samples were flushed with ethanol to quench the reaction and remove glycerol for SEM characterizations, which makes the observed thickness (less than 1 μm) of such early repair layer lower than the real one. Therefore, when the samples are gently immersed in ethanol (instead of flushing) for quenching, the thickness of new mineral layer on enamel can reach ~1.5 μm at 0–10 min (Supplementary Fig. 14).

By 30 min, the ACP nanoparticles and nanowires have completely converted into hydroxyapatite nanorods with a diameter of 20–50 nm and length of 100–300 nm (Fig. 3E1–E3, Supplementary Fig. 15), resembling those of native enamels[3]. The significant repair effect is also evidenced by a distinct contrast difference between GCPC treatment area and GCPC non-treatment area (Scheme is shown in Supplementary Fig. 15A) on each etched enamel, where the boundary is marked with an arrow in inset of Supplementary Fig. 15B. Besides, the 3D laser scanning microscope image of the surface morphology (Supplementary Fig. 15C) shows a height difference between GCPC treatment area and GCPC non-treatment area. Grazing incidence X-ray

https://doi.org/10.1038/s41467-024-54785-y

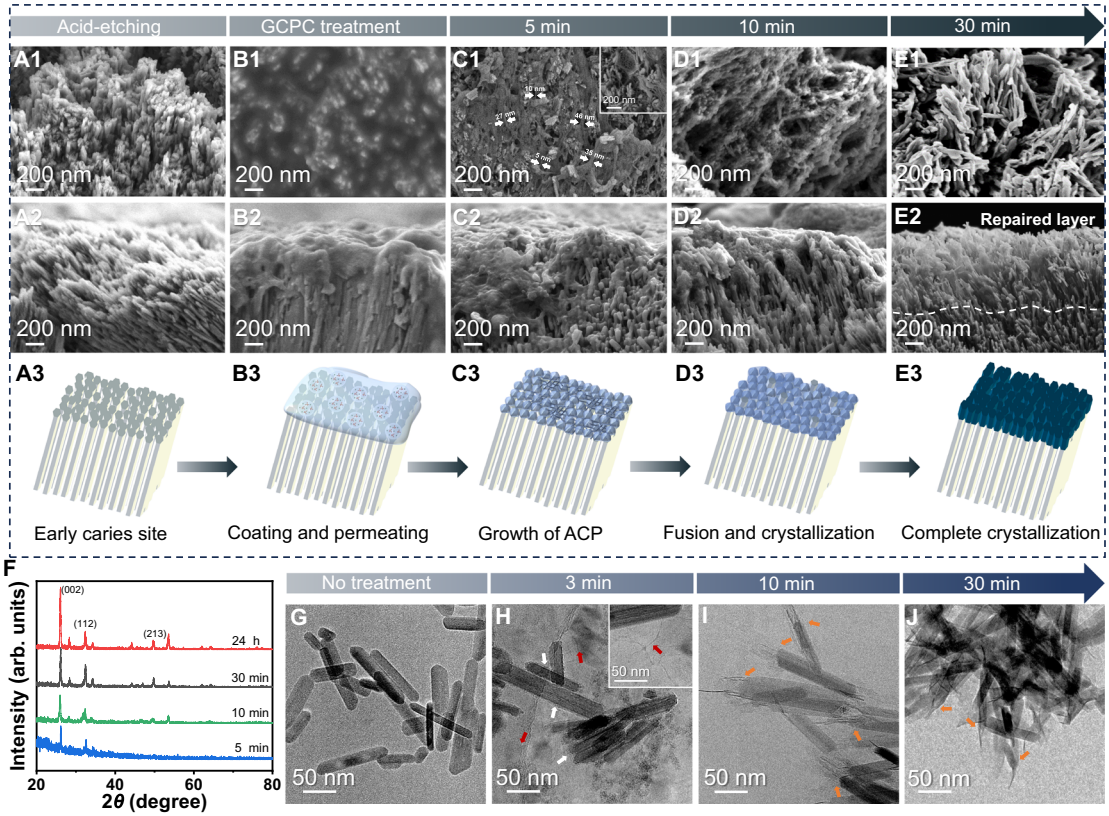

Fig. 3 | Rapid repair of demineralized enamel by GCPC in artificial saliva. A1–A3, B1–B3, C1–C3, D1–D3, E1–E3 SEM images from the top surface and cross-sectional view of etched enamel before (**A1–A2**) and after treatment for 0 min (**B1–B2**), 5 min (**C1–C2**), 10 min (**D1–D2**) and 30 min (**E1–E2**). The dashed line in E2 marks the speculated boundary between the natural enamel and the repair layer. **A3**, **B3**, **C3**, **D3** Schemes illustrating the repair performances of GCPC on etched enamels over time, which goes through enamel caries site caused by acid etching (**A3**), the coating and permeating in 0 min (**B3**), growth of ACP in 5 min (**C3**), fusion and crystallization in 10 min (**D3**) and complete crystallization in 30 min (**E3**). **F** GIXRD spectra of enamel surface repaired by GCPC for 5 min, 10 min, 30 min and 24 h. **G** TEM image of the HAP nanorods without treatment. Cryo-TEM images of the GCPC-treated HAP nanorods at 3 min (**H**) and 10 min (**I**). Clusters are indicated by white arrows and the newly formed nanowires are marked by red arrows in (**H**). **J** TEM images of the GCPC-treated HAP nanorods at 30 min. Newly formed structures at the ends of HAP nanorods are marked by orange arrows in (**I**, **J**).

diffraction (GIXRD) was conducted to further characterize the evolution of calcium phosphate layer on GCPC treated enamel surface. The weak crystalline diffractions and noisy background (Fig. 3F) indicate that GCPC generates an amorphous or very weakly crystallized calcium phosphate layer on enamel by water-triggered transformation at 5 min (the weak HAP signals on the pattern may be contributed by the enamel substrate underneath the GCPC). Then over time (from 10 to 30 min), the intensity of characteristic peak of HAP on GIXRD pattern increases, suggesting that the GCPC gradually evolves into HAP on the enamel, consistent with obversion by SEM. To determine whether the newly formed hydroxyapatite crystals were firmly attached to the enamel, ultrasonic treatment (1500 W, 40 KHz, 30 s) was performed on enamel formed by GCPC treatment in artificial saliva for 30 min. The results of SEM (Supplementary Fig. 16) show that the HAP crystals derived from GCPC remain tightly attached on the etched enamel substrate, confirming that they are indeed growing closely with the enamel rather than simply adhering to the surface.

As a comparison, the remineralization capacity of CPP-ACP paste, a normal commercial enamel remineralization product in clinic, is also tested on the caries model for the same time (30 min). Unlike GCPC, the morphology of CPP-ACP treatment area shows little difference from that of CPP-ACP free one (Supplementary Fig. 17A, the boundary is marked with an arrow in inset). Attributed to the weak repair effect in such short time, only sparse minerals adhere to the enamel (Supplementary Fig. 17B). In addition, applying the 3X-GCPC leads to a very flat, well-organized and more compact repair layer at 30 min (Supplementary Fig. 18), indicating that a higher concentration of the GCPC can improve the repair effect in vitro.

HAP nanorods, with the similar morphology and structure to the HAP crystals in natural enamel, can be used as a simplified in vitro model to study enamel remineralization[7,8]. Herein, in order to further understand the growth mechanism of HAP crystals during enamel repair by GCPC, the synthesized HAP nanorods (Fig. 3G, Supplementary Fig. 19A, B) were mixed with GCPC, then incubated in artificial saliva for a certain duration (3, 10 and 30 min). The characterization results in Fig. 3H show that, comparing to the original HAP nanorods, the ones treated by GCPC adhere clusters on the top and side (indicated by white arrows) after incubation in artificial saliva at 3 min. Furthermore, nanowires (indicated by red arrows) with the diameter of ~2 nm, similar to the size of GCPC, are also found in the solution. In addition, the constituent clusters in some sections of the nanowires (indicated by white arrows) suggest that they are probably formed by the assembly of the clusters (Supplementary Fig. 20). We note that the diameter of the nanowires in cryo-TEM images is much smaller than that in normal SEM (Fig. 3C1). It is possible that the drying process for SEM observation, which is not needed for cryo-TEM, causes the shrinkage, aggregation and fusion of the thin nanowires. At 10 min, the nanorods grow longer with newly formed minerals at their ends, instead of the sides (Fig. 3I), which is kept at 30 min (Fig. 3J). Therefore, GCPC does have an affinity to the HAP nanorods in the artificial saliva, and the new minerals originated from GCPC prefer to grow from the top (not the sides) of the nanorods. This preference essentially favors

https://doi.org/10.1038/s41467-024-54785-y

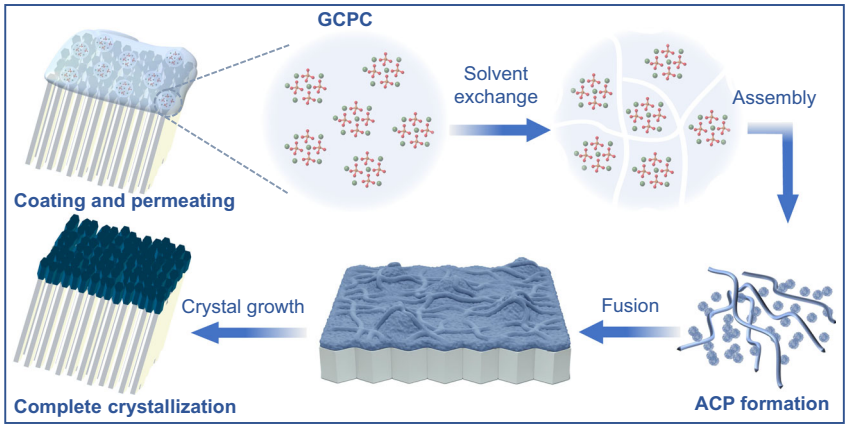

Fig. 4 | Scheme of the rapid repair process of demineralized enamel by GCPC via a water-triggered transformation. GCPC rapidly infiltrates the acid-etched enamel defects, forming ACP nanoparticles and nanowires in artificial saliva upon solvent exchange. These species are further fused and transformed into HAP nanorods, creating a repair layer on the enamel surface.

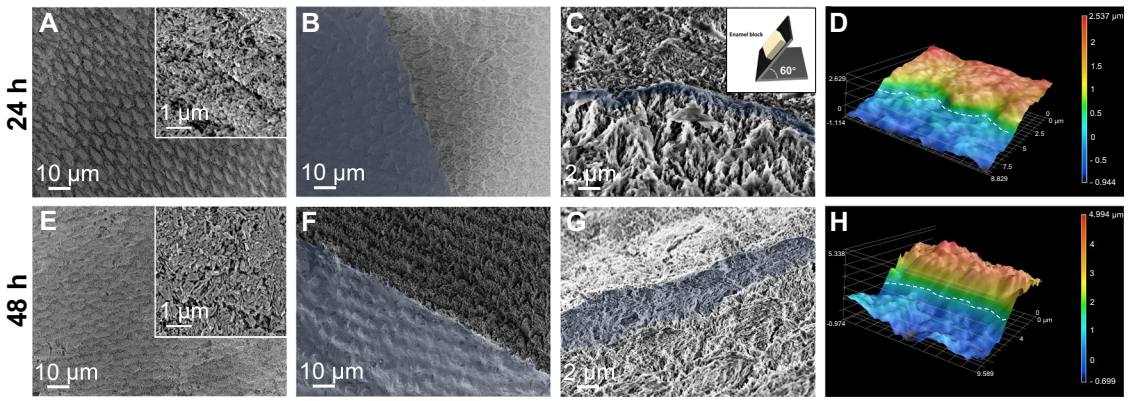

Fig. 5 | Repair of demineralized enamel using GCPC for 24 h and 48 h. SEM images of GCPC treatment areas (**A**), boundary between GCPC treatment (blue) and non-treatment areas (**B**), and the cross section (C, blue region: speculated repair layer) on etched enamel after repair for 24 h. Inset in (**C**) shows that the enamel sample is tilted to a degree of 60° for cross-sectional observation. **D** 3D laser scanning microscope image of the etched enamel surface consists of GCPC treatment (higher height) area and non-treatment (lower height) area after repair for 24 h. SEM images of the GCPC treatment areas (**E**), boundary between GCPC treatment (blue) and non-treatment areas (**F**), and the cross section (**G**, blue region: speculated repair layer) on etched enamel after repair for 48 h. **H** 3D laser scanning microscope image of the etched enamel surface consists of GCPC treatment (higher height) area and non-treatment (lower height) area after repair for 48 h.

the restoration of the demineralized enamel by GCPC, and more importantly, avoids a total disordered arrangement of the formed HAP crystals during enamel repair.

Based on the characterizations above, we propose a pathway of enamel repair by GCPC (Fig. 4). When coating GCPC on the acid etched enamel, they quickly permeate into the nano-/micro-sized defects. Meanwhile, in the artificial saliva environment, glycerol, which acts as a stabilizer in GCPC, is dissolved instantly, resulting in the formation of ACP nanoparticles and nanowires on the enamel crystals. Subsequently, the ACP nanoparticles fuse and crystallize into HAP nanorods (diameter 20–50 nm). These rod nanocrystals, as the constituent units of the repair layer, grow closely on the enamel surface. This mineral formation process exhibits a nonclassical crystallization behavior since the crystals grow by the aggregation of metastable intermediate species (e.g., clusters, particles) rather than a direct ion-by-ion attachment (classical crystallization), which has been extensively discussed in the growth of biominerals[33–35].

With prolonging the incubation to 24 h, the morphology of repair layer (i.e., HAP short rods) has no significant changes from that of 30 min, indicating that such short time (30 min) is sufficient for GCPC to complete its repair process (Fig. 5A–C). Moreover, the results of GIXRD (Fig. 3F) show that there is no significant difference in crystallinity between the specimens collected at 30 min and 24 h, supporting that nearly all of the GCPC is crystallized at 30 min. Cross-sectional view and the 3D laser scanning microscope image of the treated enamel show that the thickness of the remineralization layer is ~1 μm (Fig. 5C, D, Supplementary Fig. 21C, D). In the control sample where the etched enamel without coating GCPC is directly immersed in artificial saliva, no visible HAP crystal growth is found, indicating that artificial saliva has very weak capacity of enamel remineralization, and excluding the possibility of the enamel remineralization by artificial saliva independently during GCPC treatment (Supplementary Fig. 22). Further treating the enamel with GCPC again and culturing it in artificial saliva one more day through the same procedure (i.e., treatment with GCPC for 2 times, and incubation in artificial saliva for 48 h totally) (Fig. 5E–H) a thicker remineralization layer (3 μm) composed of HAP nanorods are formed (Fig. 5G, H, Supplementary Fig. 21E, F). This indicates that repeating the treatment with GCPC can also improve the remineralization effect.

As fluoride is able to modulate crystal orderliness by inducing a preferential needle-like crystal structure formation[36,37], we tried two ways to improve the order of the formed crystals on enamel with the aid of fluoride. First, we introduced a small quantity of NaF into artificial saliva (15 ppm, F-AS) to replace normal artificial saliva during the

https://doi.org/10.1038/s41467-024-54785-y

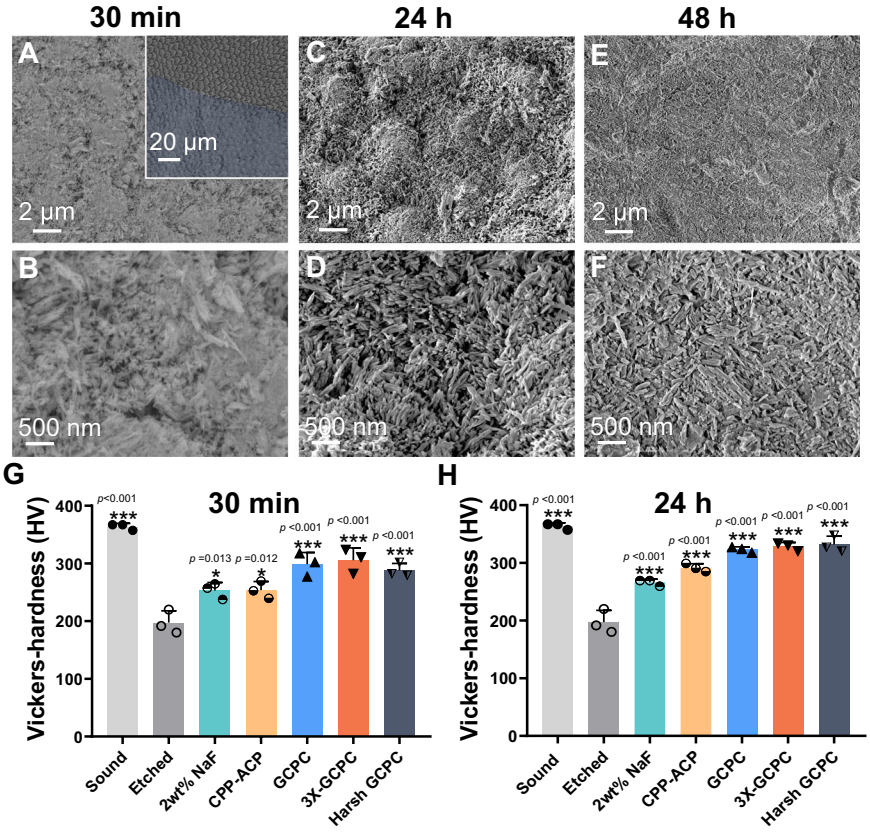

Fig. 6 | Repair of demineralized enamel using GCPC in harsh environment. SEM images of the enamel repaired by GCPC under oscillation condition (80 rpm) for 30 min (**A**, **B**), 24 h (**C**, **D**) and 48 h (**E**, **F**). Inset: the boundary between GCPC treatment (blue) and non-treatment areas. Microhardness of different enamel samples after repair for 30 min (**G**) and 24 h (**H**). Sound, etched, 2 wt% NaF, CPP-ACP, GCPC, and 3X-GCPC correspond to the samples of sound enamel, etched enamel (blank group), enamels repaired by 2 wt% NaF, CPP-ACP paste, GCPC and 3X-GCPC in static artificial saliva respectively; Harsh GCPC represents the enamel repaired by GCPC under oscillation condition. Statistical differences are assessed using one-way analysis of variance (ANOVA) and Tukey's multiple comparisons test. The asterisk (*) denotes significant differences between the indicated group and the etched group (p values higher than 0.001 are displayed above the asterisks). The error bars represent the mean ± SD for $n = 3$ independent experiments, $^{*}p < 0.05$, $^{**}p < 0.01$, $^{***}p < 0.001$; no data were excluded from the analyses.

in vitro remineralization experiment (treated by the materials but then incubated in F-AS instead of normal artificial saliva). As displayed in the SEM images of Supplementary Fig. 23, comparing to the blank group (without treatment by any materials but also incubated in F-AS for 24 h), the GCPC group can form a dense repair layer composed of highly ordered HAP crystals at 30 min and 24 h, while the crystals in CPP-ACP group still show disordered arrangement. Second, we introduced a small quantity of NaF into GCPC (0.5 ppm, F-GCPC) and subsequently conducted an in vitro remineralization experiment (treated by F-GCPC then incubated in normal artificial saliva). Similarly, enamel samples treated by F-GCPC exhibit a flat surface with the growth of dense and oriented crystals (shown in cross-sectional SEM images, Supplementary Fig. 23) as well. These findings demonstrate that, at an optimized condition (e.g., adding fluorine to regulate mineralization), GCPC is able to form more ordered crystals in the repair layers.

Since the teeth in mouth are surrounded by fluid saliva, and frequently rubbed by moving cheek and tongue, we simulated the dynamic environment in mouth to further evaluate the repair capacity of GCPC. Here, based on treatment process as above, GCPC coated samples are placed under oscillation condition (80 rpm/min) during incubating in artificial saliva. SEM images show that a dense repair layer composed of short HAP rods still forms on enamel surface in such a harsh environment within either a short (30 min) or long (24 h and 48 h) mineralization time (Fig. 6A–F). These results suggest that GCPC has a high repair efficiency in both static and dynamic environments.

As mechanical properties, especially hardness, are major contributors to normal functions of teeth, thus it is essential to evaluate them on the repaired enamels. Fig. 6G, H illustrate the microhardness of the sound, acid etched (caries model) and GCPC repaired enamels characterized by a Vickers hardness tester. The sound enamel has a hardness of 363.83 ± 5.66 HV (mean ± SD), but it is significantly weakened after acid etching with the value reduced to 197.33 ± 20.44 HV. Whereas, after a fast repair (30 min), the treatments by GCPC and 3X-GCPC greatly recover the hardness to 298.73 ± 20.34 HV and 305.67 ± 21.31 HV, which are 82.1% and 84.0% of sound enamel, respectively. These mechanical property recoveries should be attributed to the growth of compact HAP nanorods on etched enamel by remineralization. In contrast, by using conventional remineralization agents, e.g., 2 wt% NaF and CPP-ACP paste, for the same duration (30 min), the enamel hardness stays at relatively low values of 253.07 ± 13.94 HV and 253.87 ± 14.88 HV because of their poor remineralization rates. The hardness of the enamel is further improved after incubation for 24 h. Compared to 2 wt% NaF (266.07 ± 5.60 HV) and CPP-ACP paste (291.43 ± 7.11 HV), the hardness of the repaired enamel by GCPC and 3X-GCPC increases to 322.73 ± 4.99 HV (88.70% of sound enamel) and 328.30 ± 6.97 HV (90.23% of sound enamel), respectively. In addition, GCPC treated enamel also shows prominent hardness recovery under oscillation conditions that mimic the harsh dynamic oral environment. At 30 min, the hardness of enamel (Harsh GCPC in Fig. 6G) repaired in oscillator reaches to 287.90 ± 12.19 HV (79.13% of sound enamel); after 24 h, the value reaches to 331.90 ± 14.41HV (91.22% of sound enamel), the highest of among all samples. The above conclusions are consistent with the results tested by a nanoindentation (Supplementary Fig. 24), the latter of which also

https://doi.org/10.1038/s41467-024-54785-y

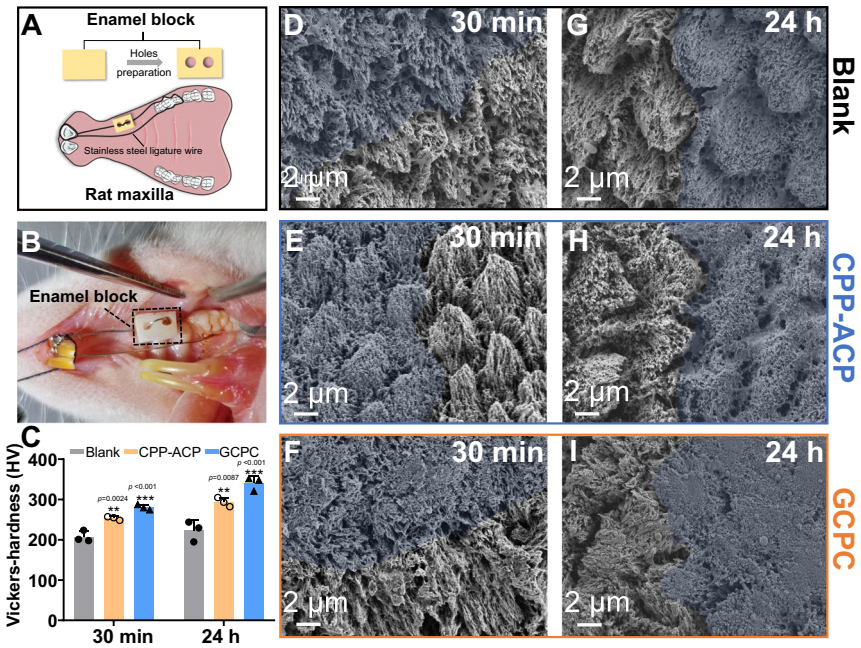

Fig. 7 | The repair of demineralized enamel in vivo. Scheme (**A**) and photograph (**B**) of vivo animal model showing the etched enamel fixed in the oral cavity of rats. **C** Microhardness of the enamels repaired by different materials in vivo for 30 min and 24 h. The error bars represent the mean ± SD for $n = 3$ independent experiments, and no data were excluded from the analyses. Statistical differences are assessed using one-way ANOVA and Tukey's multiple comparisons test. The asterisk (*) denotes significant differences between the indicated group and the blank group (p values higher than 0.001 are displayed above the asterisks). $^{**}p < 0.01$, $^{***}p < 0.001$. SEM images of the enamels repaired by deionized water (**D**), CPP-ACP paste (**E**) and GCPC (**F**) for 30 min in vivo. SEM images of the enamels repaired by deionized water (**G**), CPP-ACP paste (**H**) and GCPC (**I**) for 24 h in vivo. The blue regions represent the treatment areas.

observes the improvement of hardness and Young's modulus of enamel after treated by GCPC, better than the conventional remineralization materials/commodities, e.g., 2 wt% NaF and CPP-ACP.

Supplementary Table 1 summarizes the representative advances on enamel remineralization materials in the past 10 years, where the details of their repair performance are compared with GCPC. Among these materials, application of GCPC shows apparent advantages of rapid rate (within 30 min), effectiveness in harsh environment and easy conduct (no need for special pretreatment of enamels). Considering in the clinic practice of enamel repair, there's no need for patients to dry the tooth surface, spend additional time for material adhering, or limit too much mouth motion, these merits are beneficial for positive patient compliance and clinical promotion.

Animal study of enamel repair

Encouraged by the above results, we further applied an in vivo animal model (Fig. 7A) to ascertain the performance of the GCPC on remineralization of etched enamel by a rapidly water-triggered transformation. In our animal model, acid etched enamel blocks with half surface coated with nail varnish were fixed in the maxilla of rats where they were under the frictions from buccal and lingual muscles. Moreover, the mouths of rats provided a dynamic liquid environment containing both inorganic ions and organic molecules (Fig. 7B). Without any additional pretreatments of enamels (e.g., drying), we used micro brushes to apply GCPC, CPP-ACP paste or deionized water (blank) on enamel blocks to mimic daily oral care, then evaluate the repair effects after a certain time.

After 30 min of oral incubation, hardly any new crystals grow on the demineralized enamels treated with deionized water (Fig. 7D, Supplementary Fig. 25A, B), leading to little differences between the treated and un-treated areas. This indicates that the enamel defects could not be repaired by saliva alone in such a short time. Instead, GCPC and CPP-ACP paste treatments result in remineralization effects on the surfaces, and that of GCPC forms much more compact crystals than CPP-ACP paste (Fig. 7E, F, Supplementary Fig. 25E, F, I, J). These crystals have the morphologies of nanorods with a diameter of 50–70 nm and length of 100–300 nm. This proves that, like in vitro performance, GCPC also has a rapid repair ability in vivo via the water-triggered transformation. In contrast, CPP-ACP paste should be relatively more vulnerable than GCPC to dynamic environment of the actual mouth due to the slow repair rate. After 24 h, similar to the early stage, we can observe the densest repair layer composed of HAP nanorods on the GCPC group than the others (Fig. 7I, Supplementary Fig. 25K, L). Meanwhile, deionized water (Fig. 7G, Supplementary Fig. 25C, D) and CPP-ACP paste (Fig. 7H, Supplementary Fig. 25G, H) groups still present little difference of the morphology from the etched enamel. As shown in Supplementary Fig. 26, after high-power (1500 W, 40 KHz) ultrasonic treatment for 30 s, there is still a dense repair layer on the enamel repaired by GCPC at 30 min and 24 h in animal study, suggesting that newly formed HAP crystals are structurally integrated with enamel substrate. Contributed by the high performance of remineralization, GCPC group shows a great enamel hardness recovery in 30 min, reaching the value 280.57 ± 6.70 HV, compared with deionized water (207.53 ± 14.09 HV) and CPP-ACP paste (253.50 ± 4.73 HV) groups. Further mechanical measurements at 24 h also show that the hardness of GCPC group (340.13 ± 17.10 HV) is the highest among the characterized groups (CPP-ACP paste group: 293.47 ± 11.35 HV; deionized group: 222.73 ± 25.24 HV. Fig. 7C). These results confirm that the remineralization by GCPC does not only recover the structure of enamels, but also its mechanical properties within very short time.

Discussion

In summary, we have developed a stable ultrasmall (1–2 nm) mineral species, GCPC, and find it can perform a rapid remineralization of tooth enamel by a water-triggered transformation. As an indispensable stabilizer, glycerol effectively stabilizes GCPC with its high viscosity and affinity to the clusters, but endows it with the character of water-responsive transformation due to its miscibility with water. On the

etched enamel surface, GCPC can easily enter the nano-/micro-sized defect sites due to its small size and high permeability, then quickly repair it in the artificial saliva: with a continuous exchange between glycerol and water in high rate, GCPC forms amorphous calcium phosphate nanoparticles and nanowires in 5 min, subsequently fuse and crystallize into compact HAP nanorods on the enamel surfaces, and finish the transformation in 30 min, which is much faster than the conventional materials (hours or days). No matter in the static and oscillated environments, GCPC constructs a dense mineral repair layer ultimately and recovers the mechanical properties to the values close to that of natural enamel, which is better than conventional remineralization commodities. This biocompatible material, GCPC, is not only efficient in remineralization of etched enamels, but also advantageous in easy preparation process, low cost and simple conduction on enamel treatments, making it promising in future clinical promotion.

Methods

The research complies with all relevant ethical regulations.

Materials and chemicals

Glycerol, hydroxyethyl piperazine ethane sulfonic acid (Hepes), sodium hydroxide and deuterium oxide were purchased from Shanghai Macklin Biochemical Technology Corporation, calcium chloride ($CaCl_2$), trisodium phosphate (Na_3PO_4), magnesium chloride ($MgCl_2$), potassium chloride (KCl), phosphoric acid and potassium dihydrogen phosphate (KH_2PO_4) were purchased from Aladdin Industrial Corporation. An oral health care paste product that is commonly used in enamel clinic remineralization treatment with CPP-ACP as the active substance was commercially purchased. Acetone and sodium fluoride (NaF) were purchased from Sinopharm Chemical Reagent Co. All chemicals were used as received without further purification. Human tooth samples (premolars and third molars without caries) were extracted for clinical reasons (orthodontic treatment or removal of impacted third molars) following the standard extraction procedures at Shanghai Ninth People's Hospital, and handled with permission of Ethical Committee of Shanghai Ninth People's Hospital (Approval No.:SH9H-2021-T445-2). The teeth were temporarily stored in sterile alcohol after removal.

Preparation of GCPC

At room temperature, 1.00 mmol of Na_3PO_4 was dissolved in the glycerol-dominant solvent of 3.00 mL of deionized water and 25.00 mL of glycerol. Under vigorous stirring, 2.00 mL of aqueous solution containing 1.50 mmol $CaCl_2$ was added dropwise into it, by which the solution became turbid and formed GCPC in it. In this system, the Ca/P molar ratio was 1.5:1, and the volume content of water in solvents (water/(water+glycerol)) was 16.7 v/v%. GCPC in the preparation solution without any separation is termed GCPC solution in this paper, which has only soluble NaCl as the byproduct.

The concentrations of Na_3PO_4 and $CaCl_2$ can be tripled while other conditions kept the same as above to prepare the 3X-GCPC. 3X-GCPC in the preparation solution without any separation is termed 3X-GCPC solution in this paper.

The amount of deionized water in the calcium and phosphorus salts solution was varied in equal proportion while maintaining a total volume of 30.0 mL to prepare GCPC solution with different water contents. As for the preparation in pure glycerol, the dissolution of Na_3PO_4 and of $CaCl_2$ can be accelerated by heating at 60 °C, and other conditions were kept the same as in glycerol-dominant solution. ACP in aqueous solution was prepared in deionized water by replacing all the glycerol with the same volume of water while other conditions kept the same as above.

Preparation of GCPC-ACP

To prepare GCPC-ACP, 5.00 mL of GCPC solution (water content 16.7 v/v%) was mixed with 50.00 mL of ethanol, then the resulting precipitation was centrifuged at 8420.4 × *g*, washed with ethanol for 6 times and finally dried in an evacuated desiccator.

Molecular dynamics simulation

The partial charges of Glycerol, Ca^{2+} and PO_4^{3-} were calculated using the Gaussian 16, Revision C.01, and the 6-31+g(d,p) basis functions were applied. The OPLSS-AA force field and MKTOP were used to parameterize all atoms, such as the bond parameters, angle parameters, dihedral angles. The system1 (water solvent) includes 10 PO_4^{3-}, 15 Ca^{2+} ions and 16653 water molecules; system2 (glycerol-dominant solvent) includes 10 PO_4^{3-} molecules, 15 Ca^{2+} ions, 3423 glycerol and 2775 water molecules; and system3 (glycerol solvent) includes 10 PO_4^{3-} molecules, 15 Ca^{2+} ions and 4108 glycerol molecules. All the ions and molecules were randomly added into a simulation box ($8.000 \times 8.000 \times 8.000\ nm^3$). The model of the water molecule was TIP3P. The MD simulations were performed by the GROMACS 2022.1 software package. The steepest descent method was applied to minimize the initial energy for each system with a force tolerance of 1 kJ/ ($mol^{-1}\ nm^{-1}$) and a maximum step size of 0.002 ps before the MD calculations. In all three directions, periodic boundary conditions were imposed. The Leapfrog algorithm was used to integrate the Newtonian equation of motion. The MD simulation was processed in an NPT ensemble, and the simulation time was 20 ns. The snapshots of MD simulation results were prepared by VMD. In NPT simulations, the pressure was maintained at 1 bar by the Berendsen barostat in an isotropic manner. The temperature was maintained by the V-rescale thermostat at 298.15 K. The LINCS algorithm was performed to constrain the bond lengths of hydrogen atoms. The particle mesh Ewald (PME) with a fourth-order interpolation was used to evaluate the electrostatic interactions, and the grid spacing was 1.0 Å, whereas a cutoff of 1.0 Å was employed to calculate the shortrange van der Waals interactions.

Repair of enamel using GCPC

Preparation of artificial saliva. Artificial saliva was prepared following the report[38] using 0.07 g $CaCl_2$, 0.04 g $MgCl_2$, 2.23 g KCl, 0.54 g KH_2PO_4 and 4.76 g Hepes in 1 L of deionized water, whose pH was adjusted to 7.0 at 37 °C using NaOH solution.

Repair of demineralized enamels. Demineralized enamel, as a model of caries, was prepared by acid-etching the sound human enamel. Briefly, the dental crowns were cut with a low-speed wheel diamond saw (Model 971, JIAODA, China) into 3 × 3 × 5 mm enamel blocks and embedded in resin while exposing only the top enamel surface. The exposed enamel surfaces were polished with silicon carbide paper to remove bacterium speckle and pigment, then immersed in 37 wt% phosphoric acid for 60 s to partially demineralize the enamel. Finally, these specimens were washed with anhydrous ethanol and ultrapure water and dried at room temperature.

The demineralized enamels were treated with GCPC to evaluate its repair capacity. For each of demineralized enamel, half of its surface was coated with nail varnish as the non-treatment area, and the remaining half was treated with GCPC as the treatment area. After the nail varnish completely cured, the enamel was immersed into artificial saliva at 37 °C for 1 h to totally wet it like the teeth in oral environments. Without drying the surface, a drop of GCPC solution (a volume of 30 μL; water content 16.7 v/v%) was applied onto it using a micro brush (2.0 mm, TISEN, Huanghua Promisee Dental Co., Ltd.), then brushed for 5 s, and incubated in artificial saliva at 37 °C again for certain time. After 24 h, the samples were taken out, flushed by water to remove the unbound materials on the surface, and treated with GCPC solution again as above. After further 24 h (48 h in total), the surface was cleaned again with flushing water, and dried at room temperature.

To investigate the repair effect at early time, after incubation of GCPC solution coated enamels in artificial saliva for 5 min, 10 min and

30 min, the samples were flushed with ethanol to quench the reaction and clean the surface, then dried at room temperature for characterization. In order to characterize the formed nanowires on enamel surface at 5 min, the GCPC repaired enamels were ultrasonicated for 30 s in ethanol, then the nanowires in ethanol were collected by standing for 30 min, and dropped on carbon coated copper grid for TEM observation after being dried at room temperature.

In order to investigate the crystal orderliness of the repair layer in the presence of fluorine, a small amount of NaF was introduced in artificial saliva (to get F-AS, 15 ppm NaF) or GCPC (to get F-GCPC, 0.5 ppm NaF) for the subsequent two experiments. For the first experiment, the demineralized enamels were treated by GCPC (with CPP-ACP as a control and without any material as the blank group), and incubated in F-AS for 30 min or 24 h. For the second experiment, the demineralized enamels were coated by F-GCPC, and incubated in normal artificial saliva for 30 min or 24 h.

To compare the repair effect of GCPC with other conventional materials, NaF and a commercial product with casein phosphopeptide-amorphous calcium phosphate (CPP-ACP) as the active substance were also used to treat the demineralized enamel. For NaF treatment, demineralized enamel was placed in artificial saliva containing 2 wt% NaF; for CPP-ACP paste treatment, it was conducted via the same procedures as that of GCPC.

In addition, a harsher environment was used to investigate the repair effect. Based on the procedures above, during incubation of the GCPC coated enamel in artificial saliva at 37 °C, an oscillation at 80 rpm was applied in a thermostatic oscillator (ZHTY-50V, ZHICHU, China).

In order to explore the growth mechanism of HAP during enamel repair, HAP nanorods were mixed with GCPC solution, then incubated them in artificial saliva, and collected at a certain time point for observation by cryo-TEM directly or by TEM after washing with ethanol and dried at room temperature. The HAP nanorods were prepared via a hydrothermal reaction. Briefly, 2.317 g of $CaCl_2$ was dissolved in 250 mL of deionized water to get the solution of calcium source; 1.025 g of Na_3PO_4 and 0.887 g of Na_2HPO_4 were dissolved in 250 mL of deionized water to prepare the phosphorus source. Calcium source and phosphorus source solutions were mixed during vigorous stirring by a magnetic stirrer. Then the mixture solution was transferred into a glass bottle, sealed, and heated at 120 °C for 24 h. The products were washed with deionized water and ethanol for several times and dried at 60 °C. Next, HAP nanorods were mixed with GCPC, then incubated in artificial saliva, and collected at a certain time point for characterization.

Characterizations

The freshly prepared GCPC and GCPC after storage at room temperature for 2 weeks were characterized by spherical aberration corrected transmission electron microscope (ACTEM, JEM-ARM300F) equipped with the liquid cell holder (Protochips Poseidon 500). The relative quantification of turbidity was conducted by a microplate reader (Tecan Spark10M, Switzerland), by which 200 µL of each sample was added into a well of 96-well plates and the OD values were recorded at the wavelength of 590 nm. Repeat the test three times for each group. Dynamic light scattering (DLS, Malvern Zetasizer Nano ZS90, UK) to further determine the diameters of the formed species in pure glycerol solvent (water content 0 v/v%) and the glycerol-dominant solvent (water content 16.7 v/v%), as well as the prepared GCPC-ACP dispersed in ethanol. The compositions and structures of GCPC-ACP were characterized by Thermogravimetric-Flourier transform infrared spectroscopy (TGA-FTIR, TGA 8000-Front-Clarus 680-Clarus Sq 8 T) and X-ray diffractometer (XRD, Rigaku Ultima IV, Japan).

^{31}P liquid nuclear magnetic resonance (NMR) characterization was conducted using a nuclear magnetic resonance spectrometer (AVANCE NEO 700 MHz, Bruker) at room temperature. Water in test samples was replaced with deuterium oxide. 300 scans were accumulated for ^{31}P NMR spectra of GCPC and the recycle delay was 4 s; 32 scans were accumulated for ^{31}P NMR spectra of Na_3PO_4 glycerol solution and the recycle delay was 2 s.

Gas chromatography-mass spectrometry (GC-MS, GCMS-QP2020 NX, Japan) and Gas chromatograph (GC, Agilent 8890, USA) system coupled with headspace sampling and flame ionization detector were used to determine the content of glycerol and potential ethanol in GCPC-ACP, respectively. First, the ethanol and glycerol were dissolved in the aqueous solution. Specifically, 200.0 mg of GCPC-ACP was added into 1 mL of deionized water at 37 °C for 24 h, whereby GCPC-ACP completely crystallizes and releases glycerol and ethanol into the solution. Then, the solution was centrifuged at 11660.4 × *g* for 20 min and supernatant was collected for analysis (denoted as the GCPC-ACP extracted solution). Standard solution of glycerol was prepared by dissolving 1 mg of glycerol in 1 mL of deionized water, while that of ethanol was prepared by dissolving 2.0 ug ethanol in 1 mL of deionized water. A reported derivatization protocol[39] was used to test the content of glycerol in GCPC-ACP extracted solution. 10 µL aforementioned GCPC-ACP extracted solution and standard sample solutions were dried completely under nitrogen. Methoxyamine was added to the residue to start the methoxymation. Subsequently, the samples were trimethylsilylated by adding n-hexane and BSTFA (with 1% TMCS). An SH-I-5Sil MS capillary column (30 m × 250 µm × 0.25 µm) was used to separate compounds. GC was used to determine content of ethanol in GCPC-ACP extracted solution. 1 mL sample was sealed in vials and heated at 70 °C for 30 min in a closed system. Then, 0.5 mL gas samples were injected into the GC injection port. The oven temperature was started at 40 °C and held for 5 min, then increased to 150 °C at 20 °C /min, maintained at 150 °C for 4.5 min. Helium was used as the carrier gas at 2 mL/min. A nonpolar column (MXT-WAX, Restek, USA; 60 m × 250 µm × 0.25 µm) was used for compound separation. The content of glycerol or ethanol in standard sample and GCPC-ACP sample was determined by calculating the peak area of the same retention time in the chromatogram.

GCPC-ACP and nanowires on repaired enamel surface at 5 min were characterized by transmission electron microscopy (TEM, FEI Talos F200X, USA) and energy dispersive spectroscopy (EDS) mapping. Nanowires were collected by ultrasound irrigation of the enamel immersed in ethanol for 30 s. The synthetic HAP nanorods were characterized by XRD (Rigaku Ultima IV, Japan) and FTIR (Thermo Scientific Nicolet iS20, USA). GCPC-treated HAP nanorods at 3 and 10 min were characterized by cryogenic transmission electron microscopy (cryo-TEM, Talos F200C G2, USA), and at 30 min were characterized by transmission electron microscopy (TEM, JEM2100F, Japan).

Enamel samples covered with nail varnish were washed by acetone to remove it before SEM observation. Grazing incidence X-ray diffraction (GIXRD, Rigaku Smartlab, Japan) with a grazing incidence angle of 0.1° was used to characterize GCPC treated enamels at different time points (5, 10, 30 min and 24 h). The GCPC repaired enamels were characterized by scanning electron microscopy (Zeiss Gemini 450, Zeiss Gemini 300 and Navigator-100) and 3D laser scanning microscope (VK-X3000, Keyence, Japan). Enamels repaired by GCPC in vitro or animal study were treated by ultrasound (1500 w, 40 KHz, SCIENTZ−1500F-DZ, China) for 30 s to confirm whether new crystals grow or adhere tightly on the enamel surface. Nanoindentation (Bruker Hysitron TI980, Germany) and a Vickers hardness tester (0.490 N, 15 s; HXD-1000 TMC, China) were used to assess the surface hardness of the samples. Each one was tested for three times and the average value and standard deviation were recorded.

Cytotoxicity test

Human dental pulp stem cells (provided by Shanghai YSRIBIO industrial CO., LTD.) and human oral keratinocytes (provided by Shanghai Engineering Research Center of Tooth Restoration and Regeneration) were cultured to logarithmic phase, then inoculated into 96-well plates and 24-well plates where they were soaked in complete medium

(Dulbecco's modified Eagle's medium, Gibco, USA). The cells were incubated for 24 h to allow attachment. GCPC were incubated in complete medium with different concentrations (0, 12.5, 25, 50 mg/mL) for 24 h. The supernatants were collected by centrifugation at 3470.4 × *g* for 5 min and filtrated by syringe filter unit (SLGP033RB, Millipore), then added to each well in 24-well plates and 96-well plates. After certain intervals, CCK-8 and live/dead staining assays were conducted as follows:

Cell viability was assessed by a Cell Counting Kit-8 (CCK-8) (Beyotime, Shanghai, China) assay. Briefly, 10 μL CCK-8 solution was added to each well of 96-well plates, and incubated with the cells further for 2 h. The absorbance measurements were performed three times at the wavelength of 450 nm using a microplate reader (Tecan Spark10M, Switzerland).

Live/dead staining assay was conducted using a Calcein/PI Cell Viability/Cytotoxicity Assay Kit (Beyotime, Shanghai, China) in 24-well plates. Culture medium in the wells was removed and 250 μL Calcein/PI working solution was added (prepared according to the kit instructions) to each well. The plates were incubated at 37 °C in the darkness for 30 min, then cells were imaged by inverted fluorescent microscope (Nikon Eclipse Ti-U, Japan). Green fluorescence corresponded to live cells and red fluorescence was related to dead cells.

Animal experiments (based on female Sprague-Dawley rats)

Acid-etched enamel blocks were fixed in the maxilla of rats to evaluate the repair capacity of GCPC under in vivo mouth environments. Female Sprague-Dawley (SD) rats (8 weeks old, 200–280 g, 2 enamel block samples on each rat and 5 rats in each group) were used to conduct the animal experiments, which were approved by the Ethical Committee of Shanghai Ninth People's Hospital (No.: SH9H-2022-A40–1). Two holes were symmetrically prepared on each enamel block for fixation in the rat mouths with a stainless steel ligature (diameter of 0.10 mm). Following the experimental procedures above, the surfaces of all samples were etched in 37 wt% phosphoric acid to form artificial demineralized enamels, and half surface of each one was coated with nail varnish for comparison. One end of the stainless steel ligature was inserted into the interproximal space between the first and second maxillary molars, and the other end was connected to the upper central incisors. In this case, the enamel blocks were fixed in the anterior part of the maxilla where buccal muscles and lingual muscles moved frequently and often contacted enamel samples. Then they were treated with GCPC, CPP-ACP paste, and deionized water (blank) once a day after enamel surface was wetted by saliva. After certain intervals, the enamel samples were taken out, flushed by deionized water and dried at room temperature to assess the remineralization effect.

All experimental rats were housed in standard Specific Pathogen-Free level animal facilities, ensuring optimal environmental control. The animal facility maintained a light/dark cycle of 12 h light and 12 h dark to simulate natural circadian rhythms. Each cage contained up to two rats to ensure comfort and reduce aggressive behavior due to overcrowding. Rats had free access to water and food. For surgical interventions, experimental rats were anesthetized with 2% pentobarbital sodium to ensure that the rats experienced no pain throughout the process. Subsequently, the rats were placed in a recovery room at 26 °C and closely monitored until they were fully awake. For collecting the samples of treated enamel blocks, all rats were euthanized by carbon dioxide inhalation, ensuring a painless process.

Statistics & reproducibility

The experiments in this study were repeated three times independently with similar results unless otherwise noted. The data are presented as means ± standard deviation (SD). Statistical analyses were performed using one-way ANOVA test and Tukey's multiple comparisons test. All statistical testing was two-sided, and $p < 0.05$ was considered as statistically significant. Data analysis was conducted using GraphPad Prism Software (Version 8.0.1) and SPSS statistical software (Version 21.0).

Reporting summary

Further information on research design is available in the Nature Portfolio Reporting Summary linked to this article.

Data availability

The data that support the findings of this study are provided in the Source Data file, Supplementary Data 1, and are also available from the corresponding author upon request. The coordinates of the optimized structures are provided as source data. Source data are provided with this paper.

References

1. Bawaskar, H. S. & Bawaskar, P. H. Oral diseases: a global public health challenge. *Lancet* **395**, 185–186 (2020).
2. Moradian-Oldak, J. & George, A. Biomineralization of enamel and dentin mediated by matrix proteins. *J. Dent. Res.* **100**, 1020–1029 (2021).
3. Palmer, L. C., Newcomb, C. J., Kaltz, S. R., Spoerke, E. D. & Stupp, S. I. Biomimetic systems for hydroxyapatite mineralization inspired by bone and enamel. *Chem. Rev.* **108**, 4754–4783 (2008).
4. Du, C., Falini, G., Fermani, S., Abbott, C. & Moradian-Oldak, J. Supramolecular assembly of amelogenin nanospheres into birefringent microribbons. *Science* **307**, 1450–1454 (2005).
5. Fan, Y., Sun, Z. & Moradian-Oldak, J. Controlled remineralization of enamel in the presence of amelogenin and fluoride. *Biomaterials* **30**, 478–483 (2009).
6. Cross, K. J., Huq, N. L. & Reynolds, E. C. Casein phosphopeptides in oral health-chemistry and clinical applications. *Curr. Pharm. Des.* **13**, 793–800 (2007).
7. Wang, D. et al. Controlling enamel remineralization by amyloid-like amelogenin mimics. *Adv. Mater.* **32**, 2002080 (2020).
8. Shao, C. et al. Repair of tooth enamel by a biomimetic mineralization frontier ensuring epitaxial growth. *Sci. Adv.* **5**, eaaw9569 (2019).
9. Li, L. et al. Bio-inspired enamel repair via Glu-directed assembly of apatite nanoparticles: an approach to biomaterials with optimal characteristics. *Adv. Mater.* **23**, 4695–4701 (2011).
10. Chang, R. et al. Phosphorylated and phosphonated low-complexity protein segments for biomimetic mineralization and repair of tooth enamel. *Adv. Sci.* **9**, 2103829 (2022).
11. Habraken, W. J. et al. Ion-association complexes unite classical and non-classical theories for the biomimetic nucleation of calcium phosphate. *Nat. Commun.* **4**, 1507 (2013).
12. Gebauer, D., Kellermeier, M., Gale, J. D., Bergström, L. & Cölfen, H. Pre-nucleation clusters as solute precursors in crystallisation. *Chem. Soc. Rev.* **43**, 2348–2371 (2014).
13. Dey, A. et al. The role of prenucleation clusters in surface-induced calcium phosphate crystallization. *Nat. Mater.* **9**, 1010–1014 (2010).
14. Gower, L. B. Biomimetic model systems for investigating the amorphous precursor pathway and its role in biomineralization. *Chem. Rev.* **108**, 4551–4627 (2008).
15. Olszta, M. J. et al. Bone structure and formation: a new perspective. *Mater. Sci. Eng. R.* **58**, 77–116 (2007).
16. Veis, A. & Dorvee, J. R. Biomineralization mechanisms: a new paradigm for crystal nucleation in organic matrices. *Calcif. Tissue Int.* **93**, 307–315 (2013).
17. Onuma, K. & Ito, A. Cluster growth model for hydroxyapatite. *Chem. Mater.* **10**, 3346–3351 (1998).
18. Park, J. et al. Quantitative analysis of calcium phosphate nanocluster growth using time-of-flight medium-energy-ion-scattering spectroscopy. *ACS Cent. Sci.* **4**, 1253–1260 (2018).

19. Lotsari, A., Rajasekharan, A. K., Halvarsson, M. & Andersson, M. Transformation of amorphous calcium phosphate to bone-like apatite. *Nat. Commun.* **9**, 4170 (2018).
20. De Yoreo, J. J. et al. CRYSTAL GROWTH. Crystallization by particle attachment in synthetic, biogenic, and geologic environments. *Science* **349**, aaa6760 (2015).
21. Kim, S., Ryu, H.-S., Shin, H., Jung, H. S. & Hong, K. S. In situ observation of hydroxyapatite nanocrystal formation from amorphous calcium phosphate in calcium-rich solutions. *Mater. Chem. Phys.* **91**, 500–506 (2005).
22. Yao, S. et al. Biomineralization: from material tactics to biological strategy. *Adv. Mater.* **29**, 1605903 (2017).
23. Xiao, Z. et al. Rapid biomimetic remineralization of the demineralized enamel surface using nano-particles of amorphous calcium phosphate guided by chimaeric peptides. *Dent. Mater.* **33**, 1217–1228 (2017).
24. He, J. et al. Polyzwitterion manipulates remineralization and antibiofilm functions against dental demineralization. *ACS Nano* **16**, 3119–3134 (2022).
25. Babaie, E. et al. Polymer-Induced Liquid Precursor (PILP) remineralization of artificial and natural dentin carious lesions evaluated by nanoindentation and microcomputed tomography. *J. Dent.* **109**, 103659 (2021).
26. Zhou, C. H., Beltramini, J. N., Fan, Y. X. & Lu, G. Q. Chemoselective catalytic conversion of glycerol as a biorenewable source to valuable commodity chemicals. *Chem. Soc. Rev.* **37**, 527–549 (2008).
27. Robergs, R. A. & Griffin, S. E. Glycerol. Biochemistry, pharmacokinetics and clinical and practical applications. *Sports Med.* **26**, 145–167 (1998).
28. Gebauer, D., Gale, J. D. & Cölfen, H. Crystal nucleation and growth of inorganic ionic materials from aqueous solution: selected recent developments, and implications. *Small* **18**, 2107735 (2022).
29. He, K. et al. Revealing nanoscale mineralization pathways of hydroxyapatite using in situ liquid cell transmission electron microscopy. *Sci. Adv.* **6**, ezza7524 (2020).
30. Li, N. et al. Biomimetic inorganic-organic hybrid nanoparticles from magnesium-substituted amorphous calcium phosphate clusters and polyacrylic acid molecules. *Bioact. Mater.* **6**, 2303–2314 (2021).
31. Vecstaudza, J., Gasik, M. & Locs, J. Amorphous calcium phosphate materials: formation, structure and thermal behaviour. *J. Eur. Ceram. Soc.* **39**, 1642–1649 (2019).
32. Mu, Z. et al. Pressure-driven fusion of amorphous particles into integrated monoliths. *Science* **372**, 1466–1470 (2021).
33. Zhang, H., De Yoreo, J. J. & Banfield, J. F. A unified description of attachment-based crystal growth. *ACS Nano* **8**, 6526–6530 (2014).
34. Sun, S., Gebauer, D. & Cölfen, H. Alignment of amorphous iron oxide clusters: a non-classical mechanism for magnetite formation. *Angew. Chem. Int. Ed. Engl.* **56**, 4042–4046 (2017).
35. Jehannin, M., Rao, A. & Cölfen, H. New horizons of nonclassical crystallization. *J. Am. Chem. Soc.* **141**, 10120–10136 (2019).
36. Teerakanok, S., Zhao, M., Giordano, R. & Fan, Y. Interaction of doped magnesium, zinc and fluoride ions on hydroxyapatite crystals grown on etched human enamel. *J. Cryst. Growth* **571**, 126262 (2021).
37. Fan, Y., Sun, Z. & Moradian-Oldak, J. Effect of fluoride on the morphology of calcium phosphate crystals grown on acid-etched human enamel. *Caries Res.* **43**, 132–136 (2009).
38. Cao, G. et al. Antibacterial silver-doped calcium phosphate synthesized by an enzymatic strategy for initial caries treatment. *Ceram. Int.* **46**, 22466–22473 (2020).
39. Liu, Y. et al. An ultrasonication-assisted extraction and derivatization protocol for GC/TOFMS-based metabolite profiling. *Anal. Bioanal. Chem.* **400**, 1405–1417 (2011).

Acknowledgements

The financial support from the National Natural Science Foundation of China (31771081, F.C.; 82370941, X.C.; 52272304 B.L.), National Key R&D Program of China (2022YFE0123500, F.C.), the Science and Technology Commission of Shanghai Municipality (21ZR1449700, B.L.; 22S31903300, F.C.; 22Y11903200, X.C.), and Cross-disciplinary Research Fund of Shanghai Ninth People's Hospital, Shanghai JiaoTong University School of Medicine (JYJC202204, X.C.) are gratefully acknowledged.

Author contributions

X.C., F.C., B.L., and N.L. initiated the study. X.C., F.C., and B.L. supervised and supported the project. N.L. carried out the enamel repair and most of the characterizations. Y.D. and J.W. performed the biocompatibility experiment. N.L., H.Z. and X.X. prepared the GCPC materials. G.C. performed the microhardness tests. N.L., B.L., F.C., X.C., X.J., X.F., Z.Z., Y.Z., and J.Z. analyzed the data. X.C., F.C., B.L., and N.L. wrote the manuscript. All authors reviewed and approved the manuscript.

Competing interests

We declare the following competing interests: the Shanghai Tenth People's Hospital has filed a patent application describing the preparation and medical applications of glycerol stabilized calcium phosphate clusters (application No.: CN202110793157; author: Feng Chen and Bing-Qiang Lu; authors of the paper which are not authors of the patent have no financial or non-financial competing interest; status: awarded).

Additional information

Supplementary information The online version contains supplementary material available at https://doi.org/10.1038/s41467-024-54785-y.

Correspondence and requests for materials should be addressed to Bing-Qiang Lu, Feng Chen or Xi Chen.

Peer review information *Nature Communications* thanks the anonymous reviewers for their contribution to the peer review of this work. A peer review file is available.